Analytical analyses of stress transfer in fibre-reinforced composites with bonded and debonded fibre ends

CHUN-HWAY HSUEH
Metals and Ceramics Division, Oak Ridge National Laboratory Oak Ridge, Tennessee 37831, USA

The elastic stress transfer from the matrix to the fibre is analysed analytically for fibre-reinforced composites when the loading direction is parallel to the fibre axis. The fibres with bonded lateral interfaces and (1) debonded and (2) bonded ends are considered in the present study. For the case of debonded ends, the present solutions contain refinements of the previously derived analytical solutions. For the case of bonded ends, unlike the numerical solutions derived previously, the present analytical solutions are ready to be used for further analyses. The results show that the stress transfer is more effective when the fibre has higher Young's modulus or longer length. Also, compared to the debonded ends case, the stress transfer is more effective and the stress distribution is more uniform when the ends are bonded to the matrix.

1. Introduction

Fibre-reinforced composites have been used extensively and are contemplated for future applications as they offer a means of achieving superior mechanical properties [1–3]. These composites often contain discontinuous strong fibres where at least a portion of the fibres have their longitudinal axes parallel to the loading direction to achieve a substantial reinforcement. Tensile stresses applied on the composites can be transferred from the matrix to fibres by shear at the fibre–matrix interface [4–8] and, when the fibre ends are bonded to the matrix, through the ends of the fibre. This stress transfer plays an important role in controlling the mechanical properties of the composites.

Experimental techniques and theoretical analyses have previously been developed to study the stress transfer phenomenon. Experimentally, a photoelastic technique was used to evaluate the two-dimensional stress in a sheet of resin containing a rectangular Dural bar [9, 10]. Existence of high shear stress near the ends of the bar was confirmed [9, 10]. Theoretically, a single fibre with finite length embedded in a coaxial cylindrical matrix was adopted as a model system for stress analyses [11–14]. Analytical solutions of the stress transfer have been derived; however, the solutions were limited to the case where the ends of the fibre are debonded from the matrix [4, 5, 11]. Analyses considering bonded fibre ends have been performed numerically by using polynomial approximations [12], finite element analyses [13] or finite difference analyses [14].

The purposes of the present study are to refine the analytical analyses for the case of debonded fibre ends [4, 11], and to develop analytical solutions for the case of bonded ones. These are achieved by using the same model system of a single-fibre reinforced composite as that used by previous researchers [11–14], and by adopting an analytical technique similar to the one used for the fibre pullout problem [15]. The differences between the solutions for bonded and debonded fibre ends are revealed, the parameters controlling the stress transfer are studied, and the critical fibre length for effective stress transfer is discussed. Also, the present results are compared with some of the previous results [11, 14].

2. Analytical analyses

The geometry of a shear-lag model used in previous studies [11–14] is adopted in the present study. A fibre with radius, a, and length $2l$, is embedded in a coaxial cylindrical matrix with an outer radius, b, and an infinite length. As shown in Fig. 1, r is the distance from the fibre axis, and z is the direction parallel to the fibre axis. An axial tensile stress, σ_0, which is parallel to the fibre axis, is remotely applied to the matrix. It is assumed that both the fibre and the matrix are isotropically elastic and that the bonded fibre–matrix interface (at $r = a$) transfers stresses from the matrix to the fibre by interfacial shear, τ_a, without any sliding between the two components.

The derivations of the analytical solutions for the stress transfer problem in Fig. 1 are similar to those recently derived for the fibre pullout problem [15]. The calculational procedures are listed in the Appendix and the general solution for the axial stress distribution in the fibre, σ_f, is (see Equation A13)

$$\sigma_f = \frac{b^2 E_f \sigma_0}{a^2 E_f + (b^2 - a^2) E_m} + A \exp(\alpha z) + B \exp(-\alpha z) \quad (1)$$

0022–2461/89 $03.00 + .12

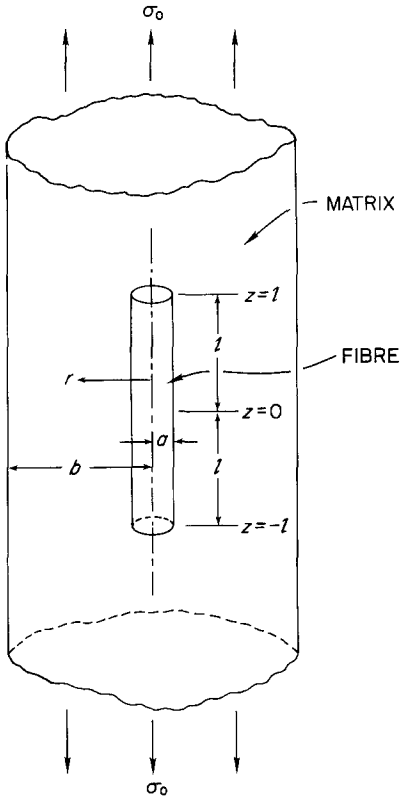

Figure 1 A schematic drawing showing the idealized shear-lag model used in the present study to analyse the stress transfer problem for fibre-reinforced composites.

where α is defined by Equation A14, E is Young's modulus, and the subscripts f and m denote the fibre and the matrix, respectively. The stress distribution in the fibre (Equation 1) is contingent upon the determination of the coefficients, A and B. Depending upon the boundary condition at the ends of the fibre, the solutions of A and B and hence the stress transfer in the system (Fig. 1) can be determined. The solutions for debonded and bonded fibre ends are considered in the following analyses.

2.1. Debonded fibre ends

When the ends of the fibre are debonded from the matrix during tensile loading, stresses cannot be transferred through the ends, i.e.

$$\sigma_f = 0 \tag{2}$$

at $z = \pm l$. Solution of Equation 1, subject to the boundary condition in Equation 2, is

$$A = B = \frac{-b^2 E_f \sigma_0}{a^2 E_f + (b^2 - a^2) E_m} \times [\exp(\alpha l) + \exp(-\alpha l)]^{-1}. \tag{3}$$

The solutions for the stress transfer (Equations 1 and A15) are hence complete.

By assuming that the stress gradient in the fibre is proportional to the difference between the axial displacement of the fibre and that of the matrix at the same point if the fibre were absent, the analytical solution of σ_f for the case of debonded fibre ends has been derived previously by Cox [11], such that

$$\sigma_f = \varepsilon E_f \left[1 - \frac{\cosh(\beta z)}{\cosh(\beta l)}\right] \tag{4}$$

where ε is the applied axial strain in the matrix and β is given by

$$\beta = \frac{1}{a}\left[\frac{E_m}{E_f(1 + \nu_m)\ln(b/a)}\right]^{1/2} \tag{5}$$

Comparison of Equations A14 and 5 shows that, when $b^2/a^2 \gg 1$, the coefficient, α, in Equation 1 can be simplified and equals β in Equation 4. Furthermore, if the strain in the matrix, ε, in Equation 4 is considered as the uniform axial strain in the composite, ε_0, when the fibre is infinitely long, then

$$\varepsilon = \varepsilon_0 = \frac{b^2 \sigma_0}{a^2 E_f + (b^2 - a^2) E_m} \tag{6}$$

The present solution (Equation 1) becomes identical to the previous one (Equation 4) derived by Cox [11] for the case of debonded fibre ends.

2.2. Bonded fibre ends

When the ends are bonded to the matrix, stress can also be transferred from the matrix to the fibre through continuity at the ends. The boundary condition (Equation 2) is trivial when the ends are debonded. However, the boundary condition is currently ambiguous when the ends are debonded. In the solutions obtained by polynomial approximations [12], a constant axial stress or displacement is assumed in the matrix at the cross-section corresponding to the fibre ends. In the solutions obtained by finite element analyses [13], a uniform axial displacement is adopted at one end of the matrix. In the case of finite difference analyses [14], the lattice in the composite is strained by a constant amount; then, the technique of overrelaxation or block relaxation is used to calculate the displacement in the equilibrium condition.

Instead of defining the exact boundary condition for bonded ends, the present study seeks an alternative boundary condition in an approximate manner, such that analytical solutions can be obtained. It is noted that within the range, $-l \leqslant z \leqslant l$ and $r \leqslant b$, the least perturbed positions (due to the presence of the fibre) are located at $z = \pm l, r = b$. Hence, stresses at these positions are assumed to be unperturbed and equal to the applied stress, such that

$$\sigma_b = \sigma_0 \tag{7}$$

at $z = \pm l$, where σ_b is the axial stress in the matrix at the outer surface ($r = b$). This assumption (Equation 7) is deemed to be appropriate when the fibre is surrounded by a relatively large matrix (e.g. $b/a > 5$). Solution of Equations 1 and A10 subject to this boundary condition (Equation 7) yield

$$A = B = \frac{a^2(E_m - E_f)\sigma_0}{a^2 E_f + (b^2 - a^2) E_m}\left[\frac{b^2 - a^2}{2\ln(b/a)} - b^2\right] \times \left[\left(a^2 - \frac{b^2 - a^2}{2\ln(b/a)}\right)\frac{E_m}{E_f} - a^2\right]^{-1} \times [\exp(\alpha l) + \exp(-\alpha l)]^{-1} \tag{8}$$

Furthermore, when the fibre and the matrix have the same Young's modulus, Equation 8 can be reduced to $A = B = 0$, and the axial stress in the fibre (Equation 1) becomes uniform and equals the applied stress (i.e. $\sigma_f = \sigma_0$ when $E_f = E_m$).

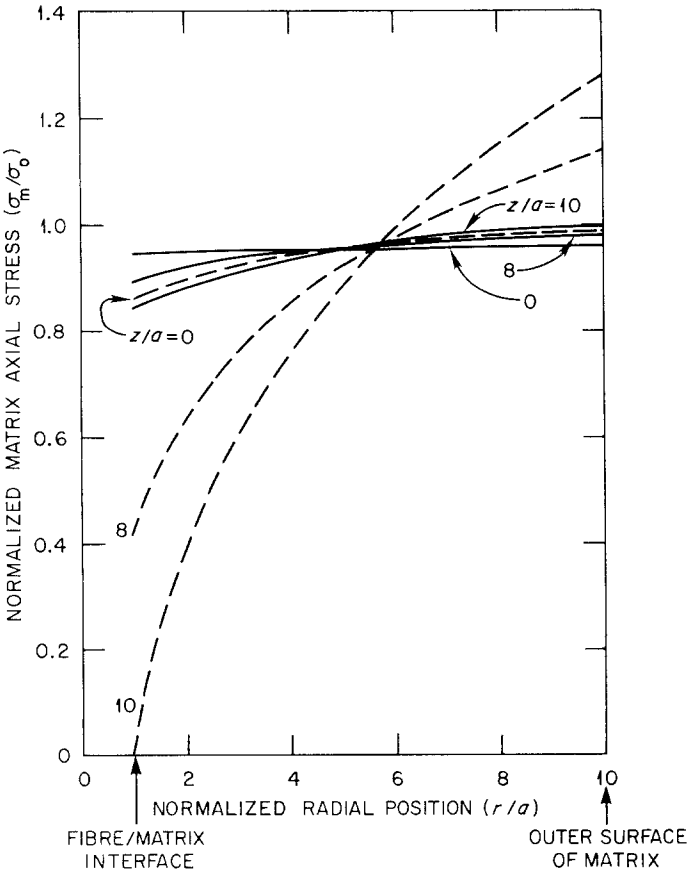

Figure 2 Normalized axial stress in the matrix as a function of normalized radial position, r/a, at cross-sections located at $z/a = 0$, 8 and 10 for $E_f/E_m = 5$, $\nu_m = 0.35$, $b/a = 10$ and $l/a = 10$: (——) bonded fibre ends, (– – –) debonded fibre ends.

3. Results

Unless noted otherwise, the present results are computed using $E_f/E_m = 5$, Poisson's ratio of the matrix, $\nu_m = 0.35$, $b/a = 10$ and $l/a = 10$ for bonded and debonded fibre ends to elucidate the essential trends of the stress transfer pheonomenon. Firstly, the perturbation of the stress distribution in the matrix due to the presence of the fibre is revealed. Then, the effects of the elastic constants of the fibre and the matrix, the dimension of the matrix, and the length of the fibre on the stress transfer are studied. Finally, the critical fibre length for effective stress transfer is discussed.

Because the axial and interfacial shear stresses are, respectively, an even and an odd function of z (see Equations 1 and A15), the plots of the stress distribution along the fibre length are shown in this paper for $z \geqslant 0$. Also, the present results are compared with the existing results [11, 14].

3.1. Perturbation of stress distributions in the matrix

The axial stress distribution in the matrix at cross-sections of the shear-lag model (i.e. along the radial direction) are plotted for axial positions $z/a = 0$, 8 and 10 in Fig. 2. The stress distribution in the matrix is non-uniform due to the presence of the fibre. At the axial position corresponding to the fibre ends (i.e. at $z = l = 10a$), the stress is the most non-uniform. The stress becomes more uniform as the distance from the ends of the fibre increases (i.e. as z decreases in Fig. 2). Compared with the debonded fibre ends case, the stress in the matrix is more uniform when the fibre ends are bonded to the matrix (Fig. 2).

3.2. Effects of elastic constants on stress transfer

The normalized axial stress in the fibre and the normalized interfacial shear stress as a function of the axial position are shown in Fig. 3 for $E_f/E_m = 2$ and 5. The stress transfer from the matrix to the fibre increases with the increase in the ratio of E_f/E_m. Also, compared with the debonded ends case, the stress transfer is more effective when the ends are bonded as shown by higher axial stresses in the fibre for the bonded case in Fig. 3a. Unlike the case of debonded ends, the axial stress in the fibre has a finite value, indicating stress transfer occurs at the fibre ends when they are bonded (Fig. 3a). With the interfacial shear stress being proportional to the axial stress gradient in the fibre (see Equation A11), the interfacial shear stress becomes higher when E_f/E_m is increased or the fibre ends are debonded (Fig. 3b). The higher interfacial shear stress in the debonded ends case than the bonded ends case has also been concluded from the experimental measurement [9] and the finite element analyses [13]. The interfacial shear stress has a maximum value, $\hat{\tau}_a$, at the fibre ends and decreases to zero in the middle of the length of the fibre (Fig. 3b).

Comparison between the present model and the existing model [11] for the case of debonded ends is shown in Fig. 4, where the normalized maximum interfacial shear stress, $\hat{\tau}_a/\sigma_0$, is plotted as a function of the normalized radius of the matrix, b/a, for $E_f/E_m = 5$ and 10. The maximum interfacial shear stress predicted from the present model is higher than the existing model [11]. However, the difference decreases when b/a increases or E_f/E_m decreases

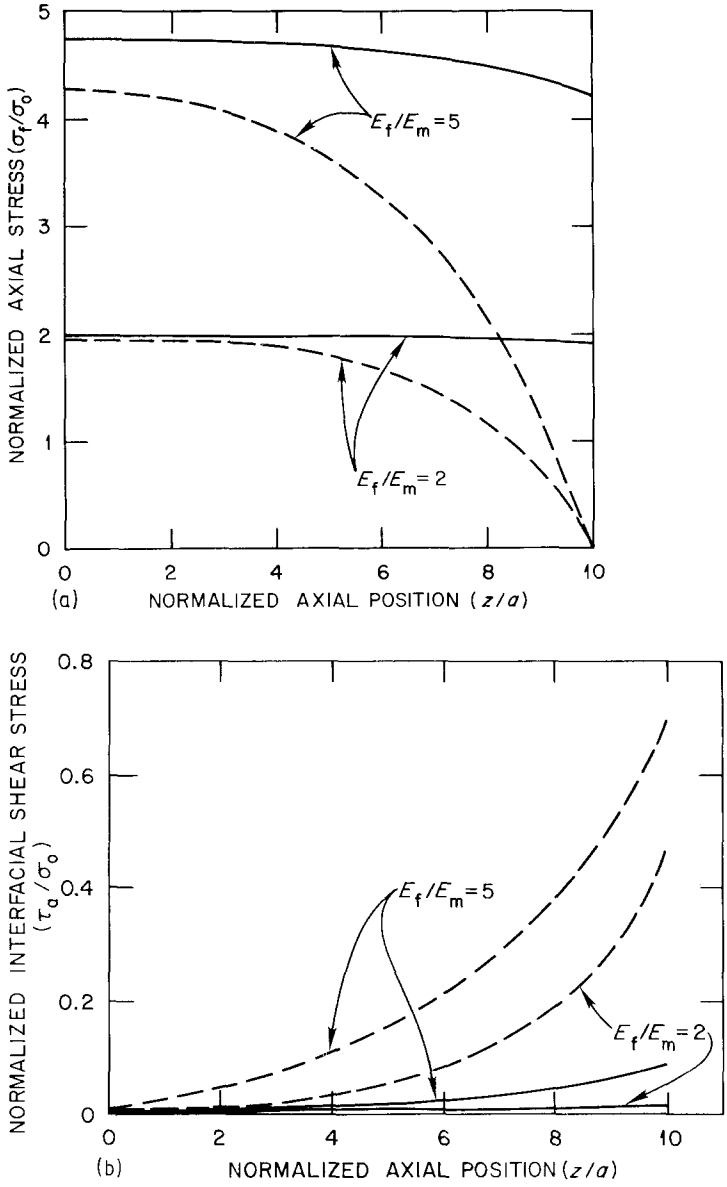

Figure 3 (a) Normalized axial stress in the fibre, and (b) normalized interfacial shear stress as a function of normalized axial position for $E_f/E_m = 2$ and 5: (——) bonded ends, (– – –) debonded ends.

(Fig. 4). For the case of bonded ends, the axial strain in the fibre, $\varepsilon_f (= dw_f/dz)$, normalized by the uniform axial strain in the composite, ε_0 (Equation 6), is plotted in Fig. 5a for $b/a = 11$ and $l/a = 25$ at different ratios of E_f/E_m. The axial strain in the fibre is less than that in the composite (i.e. $\varepsilon_f/\varepsilon_0 \leqslant 1$) and decreases with increasing E_f/E_m. This trend is consistent with the finite difference results [14]. However, the axial strains at the ends of the fibre predicted from the present model are higher than the finite difference results [14]. The interfacial shear stress distribution along the fibre length is plotted in Fig. 5b (with $b/a = 11$, $l/a = 25$ and $E_f/E_m = 20$) for the cases of bonded and debonded ends from the present analyses, of debonded ends based on Cox's analytical solutions [11], and of bonded ends derived from the finite difference results [14]. The difference between the present and the existing results [11] is small for the case of debonded ends; however,

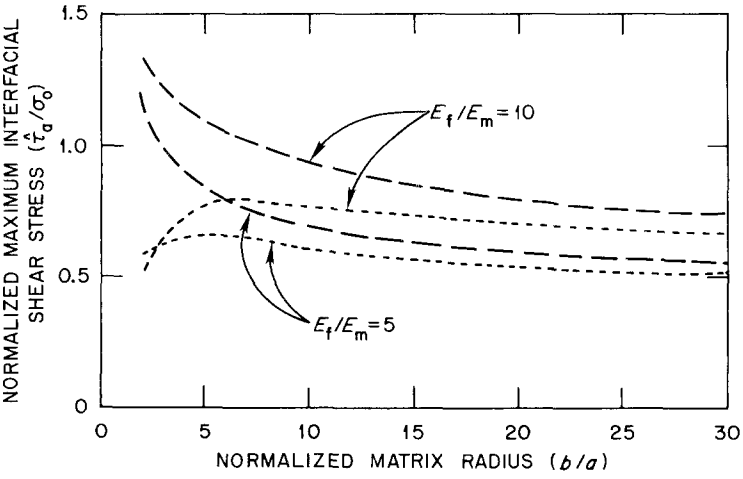

Figure 4 Normalized maximum interfacial shear stress as a function of normalized matrix radius, b/a, for the debonded ends case and $E_f/E_m = 5$ and 10: (– – –) present results, (· · ·) Cox [11].

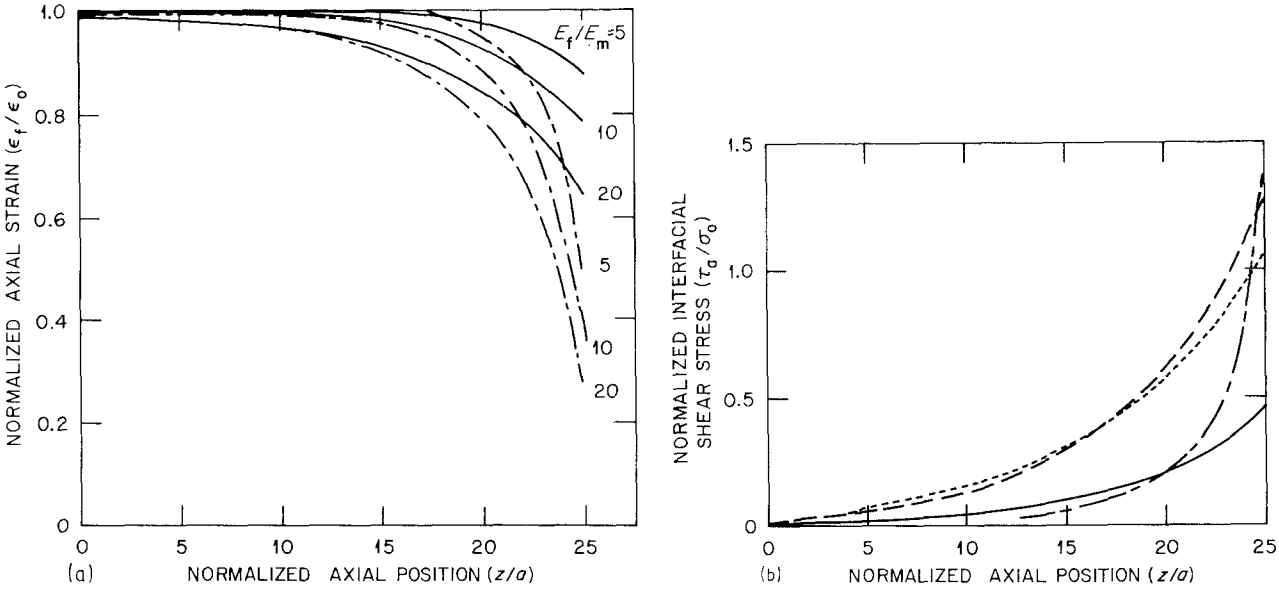

Figure 5 (a) Normalized axial strain in the fibre as a function of normalized axial position at different ratios of E_f/E_m and (b) normalized interfacial shear stress as a function of normalized axial position at $E_f/E_m = 20$ for $b/a = 11$ and $l/a = 25$: (——) present results for bonded ends, (— — —) present results for debonded ends, (— · —) finite difference results for bonded ends [14], (. . .) Cox's results for debonded ends [11].

the interfacial shear stresses at the ends predicted from the present model are much smaller than the finite difference result [14] for the case of bonded ends (Fig. 5b).

The effect of Poisson's ratio of the matrix, ν_m, on the stress transfer, σ_f, is shown in Fig. 6 by assuming arbitrarily that ν_m equals 0 and 0.5. The stress transfer becomes less effective as ν_m increases; however, this effect is negligible when the fibre ends are bonded to the matrix.

3.3. Effects of the matrix dimension

The effect of the relative radius of the matrix, b/a, on σ_f is shown in Fig. 7a. When the ends are bonded, the stress transfer is more effective and the axial stress distribution is more uniform as b/a increases. This trend is consistent with the finite difference results that an increase in the matrix radius leads to higher efficiency of stress transfer [14]. The axial stresses in the fibre at the middle and the ends (i.e. $\sigma_f(0)$ and $\sigma_f(l)$) are shown in Fig. 7b. For bonded ends case, $\sigma_f(0)$ and $\sigma_f(l)$ increase and their difference decreases as b/a increases. The increasing uniformity of σ_f can be observed from the decrease of the difference between $\sigma_f(0)$ and $\sigma_f(l)$ as b/a increases. For debonded ends case, $\sigma_f(l)$ equals 0; however, $\sigma_f(0)$ shows an initial increase and then decreases to approach an asymptote as b/a increases (Fig. 7b).

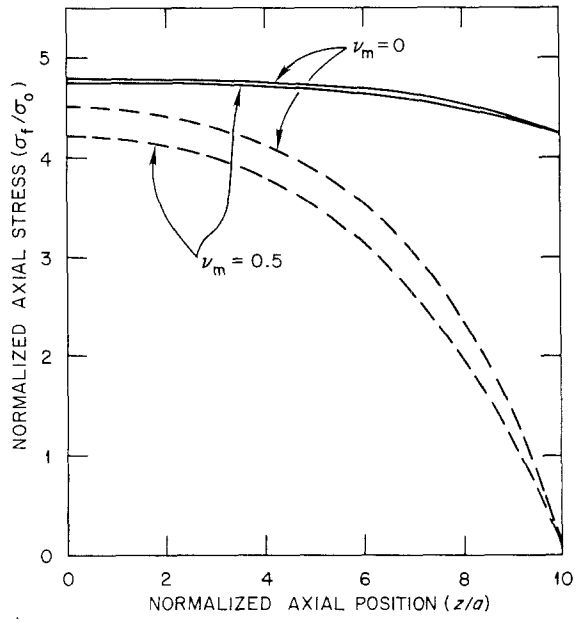

Figure 6 Normalized axial stress in the fibre as a function of normalized axial position for Poisson's ratio of the matrix $\nu_m = 0$ and 0.5: (——) bonded ends, (— — —) debonded ends.

3.4. Effects of the aspect ratio of the fibre on stress transfer and the critical fibre length for effective stress transfer

The effect of the aspect ratio of the fibre, l/a, on σ_f is shown in Fig. 8. The effectiveness in the stress transfer increases with the increase in the l/a ratio. A critical fibre length, l_c, has been defined, such that at this critical fibre length, the maximum fibre strain (i.e. the fibre strain at $z = 0$) equals 97% of that for an infinitely long fibre [14]. The normalized critical fibre length as a function of the Young's modulus ratio, E_f/E_m, is shown in Fig. 9, such that l_c/a increases with the increase in E_f/E_m. Compared with the case of bonded ends, the critical fibre length is longer in the case of the debonded ends. However, the linear relation between l_c/a and E_f/E_m derived from the finite differnce analyses [14] is not found in the present study.

4. Discussion

The present study has derived simple analytical solutions of the elastic stress transfer from the matrix to the fibre for fibre-reinforced composites with bonded and debonded fibre ends when the tensile loading direction is parallel to the fibre axis. The presence of a stress singularity at the sharp corner of the fibre ends is avoided in the present study by using the simplified

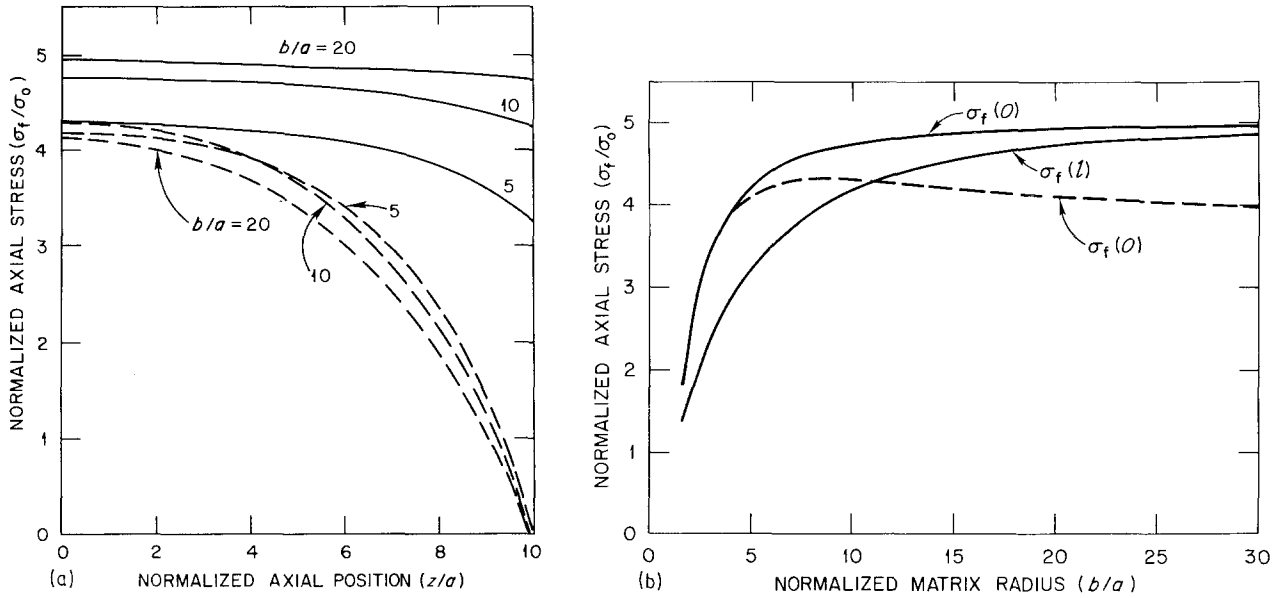

Figure 7 (a) Normalized axial stress in the fibre as a function of normalized axial position at different ratios of b/a, and (b) normalized axial stresses at the middle and ends of the fibre, $\sigma_f(0)$ and $\sigma_f(l)$, as a function of normalized matrix radius, b/a: (——) bonded ends, (– – –) debonded ends.

assumptions (e.g. Equation A1 and the condition that the axial displacement in the fibre is independent of the radial coordinate). The same assumptions have been used in a previous paper to establish the constitutive equation for the fibre pullout problem [15], and the results derived therein [15] are in excellent agreement with the rigorous numerical solutions [16]. This provides credence to the present analytical results obtained for the stress transfer problem.

Analytical solutions for the stress transfer are obtained by solving the constitutive equaiton (i.e. Equation A12) subject to the boundary conditions. When the fibre ends are debonded from the matrix, the boundary condition (Equation 2) is trivial, and the analytical solution can be derived readily. Compared with the existing analytical solutions by Cox [11], the present solutions yield higher interfacial shear stresses at the ends of the fibre; however, the difference decreases as E_f/E_m decreases or b/a increases (Fig. 3). The interfacial shear stresses at the ends derived from finite element analyses for debonded ends case [13] are also higher than those derived from Cox's solutions.

When the fibre ends are bonded to the matrix during loading, the analytical solution in the present study is achieved by using a simplified boundary condition (Equation 7), which is expected to be appropriate when b/a is large (> 5). Compared with the finite difference results [14], the same trends of stress transfer phenomena (i.e. the dependence on the Young's modulus, the fibre length and the matrix dimension) are obtained in the present analytical solutions. However, the interfacial shear stresses at the ends predicted here are much less than those obtained from the finite difference analyses [14] (see Fig. 5b).

The stress transfer behaviour has been evaluated from the photoelastic technique [9, 10]; however, its two-dimensional results make the comparison with the three-dimensional theoretical analyses difficult. The predicted low interfacial shear stresses at the ends (compared with the finite difference results) for bonded ends case obtained by the present analytical scheme may be due to the simplified boundary condition assumed in deriving the solutions. Considering the small perturbation of $\sigma_b(\pm l)$ (i.e. stress in the matrix at $r = b$ and $z = \pm l$) due to the presence of the strong fibre, $\sigma_b(\pm l)$ should be slightly lower than the applied stress, σ_0, because the stress transfer at the fibre ends is higher than σ_0. Substituting the boundary condition

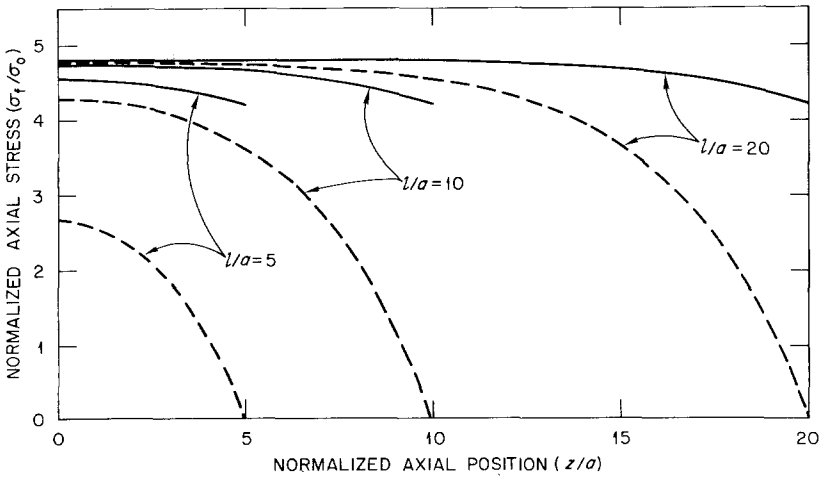

Figure 8 Normalized axial stress in the fibre as a function of normalized axial position at different values of the aspect ratio of the fibre, l/a: (——) bonded ends, (– – –) debonded ends.

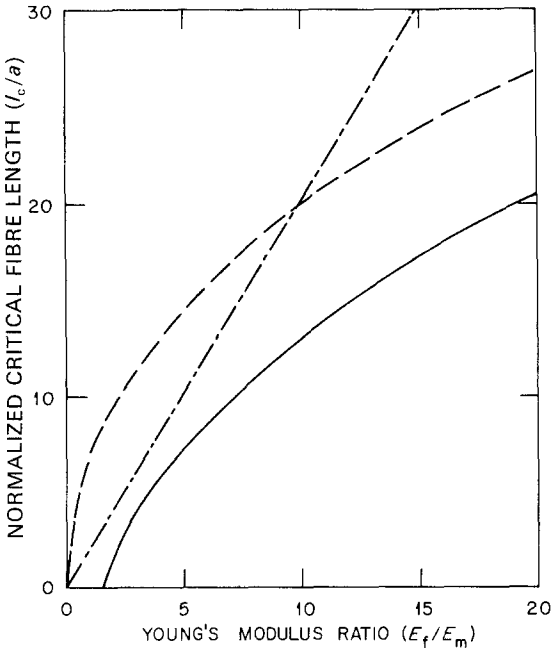

Figure 9 Normalized critical fibre length, l_c/a, as a function of the Young's modulus ratio, E_f/E_m: (——) present results for bonded ends, (– – –) present results for debonded ends, (- - -) finite difference results for bonded ends [14].

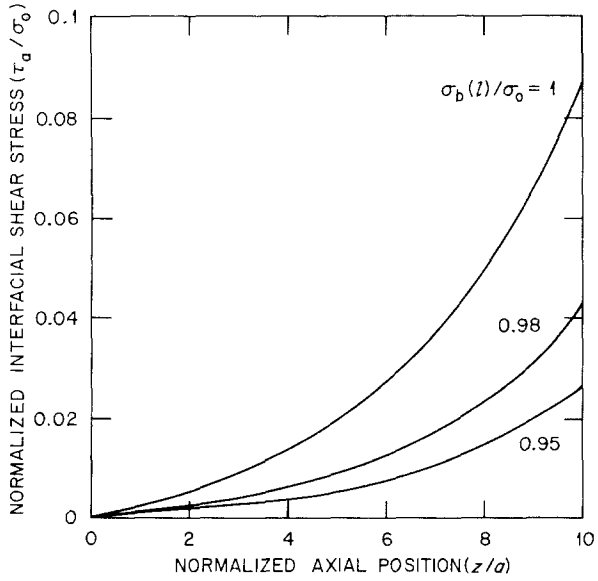

Figure 10 Normalized interfacial shear stress as a function of normalized axial position for bonded ends case with the boundary condition $\sigma_b(\pm l)/\sigma_0 = 0.95$, 0.98 and 1.

in Equation 7 by $\sigma_b(\pm l) = n\sigma_0$ where $n \lesssim 1$, the interfacial shear stresses are shown in Fig. 10 for $n = 0.95$ and 0.98 as examples to denote the small perturbation. Fig. 10 shows that the interfacial shear stress decreases as n decreases. Hence, high values of the interfacial shear stresses at the ends from the finite difference results cannot be concluded from the present analytical analyses for the bonded ends case. However, the present analytical solution for the case of bonded ends is preliminary; better boundary conditions and hence more comprehensive analytical solutions are hoped to emerge in the future.

The present results show that compared with the debonded ends case, the stress transfer is more effective and the axial stress distribution is more uniform when the ends are bonded. For debonded ends, the stress cannot be transferred across the end faces and this is partially compensated for by increasing the portion of stress transfer by interfacial shear along the fibre length [9], which in turn, results in a higher interfacial shear stress than the bonded ends case. The effect of Poisson's ratio of the fibre, ν_f, on the stress transfer is not shown in the present study and is expected to be negligible; however, when the composite has a frictional interface at the fibre–matrix interface (i.e. at $r = a$), this effect becomes important [7, 8].

With the definition of the critical fibre length, a linear relation between the critical fibre length and the Young's modulus ratio, E_f/E_m, has been concluded from the finite difference analyses [14]. The present study yields the non-linear result. Also, when the fibre ends are bonded to the matrix, the curve intercepts the x-axis at a value higher than 1 (i.e. $E_f/E_m > 1$ when $l_c/a = 0$ for bonded ends case in Fig. 8). This can be visualized because the axial strain in a discontinuous fibre is always equal to that of an infinite long fibre when $E_f = E_m$ (i.e. $\varepsilon_f/\varepsilon_0 = 1$ when $E_f/E_m = 1$). The curve where l_c/a against E_f/E_m is linear and passes through the origin, derived from the finite difference results [14], deserves further considerations.

Appendix: derivation of the constitutive equation governing stress transfer

When the fibre–matrix interface is subject to a shear stress, τ_a, the shear stress inside the matrix, τ_m, is inversely proportional to the distance from the fibre axis, such that [4, 5, 17]

$$\tau_m = a\tau_a/r \tag{A1}$$

Also, the shear stress in the matrix can be expressed as

$$\tau_m = \frac{E_m}{2(1 + \nu_m)} \frac{dw_m}{dr} \tag{A2}$$

where w_m is the displacement of the matrix element in the axial direction and E_m and ν_m are Young's modulus and Poisson's ratio of the matrix, respectively.

Combination of Equations A1 and A2, and integration give

$$\tau_m = \frac{(w_b - w_a)E_m}{2r(1 + \nu_m) \ln (b/a)} \tag{A3}$$

$$\tau_a = \frac{(w_b - w_a)E_m}{2a(1 + \nu_m) \ln (b/a)} \tag{A4}$$

where w_a and w_b are the axial displacement at the inner ($r = a$) and at the outer surfaces ($r = b$) of the matrix, respectively. The axial stresses in the fibre, σ_f, and in the matrix, σ_m, can be related to axial displacements by

$$\sigma_f = E_f \frac{dw_f}{dz} \tag{A5}$$

$$\sigma_m = E_m \frac{dw_m}{dz} \tag{A6}$$

where E_f and w_f are Young's modulus and the axial displacement of the fibre, respectively. Furthermore, for a thin fibre, the axial displacement in the fibre can

be assumed to be independent of the radial position, and identical to the axial displacement of the matrix at $r = a$ (i.e. $w_f = w_a$) to satisfy the continuity condition at the bonded fibre–matrix interface.

The axial displacment in the matrix, w_m, can be derived from Equations A2 and A4, such that

$$w_m = w_a + (w_b - w_a) \ln (r/a)/\ln (b/a). \quad \text{(A7)}$$

Substitution of w_m into equation A6 gives

$$\sigma_m = \frac{E_m}{E_f}\sigma_f + \left(\sigma_b - \frac{E_m}{E_f}\sigma_f\right)\frac{\ln (r/a)}{\ln (b/a)} \quad \text{(A8)}$$

where $\sigma_b (= E_m dw_b/dz)$ is the axial stress of the matrix at the outer surface ($r = b$). Also, mechanical equilibrium of the external load and the internal stress distributions requires

$$a^2\sigma_f + 2\int_a^b r\sigma_m \, dr = b^2\sigma_0 \quad \text{(A9)}$$

Solution of Equations A8 and A9 gives

$$\sigma_b = \left\{b^2\sigma_0 + \left[\left(a^2 - \frac{b^2 - a^2}{2 \ln (b/a)}\right)\frac{E_m}{E_f} - a^2\right]\sigma_f\right\} \Bigg/ \left[b^2 - \frac{b^2 - a^2}{2 \ln (b/a)}\right] \quad \text{(A10)}$$

Because the stress transferred from the matrix to the fibre through the interfacial shear stress (τ_a), equilibrium between τ_a and the axial stress in the fibre, σ_f, requires [4, 5, 17]

$$\frac{d\sigma_f}{dz} = \frac{-2\tau_a}{a} \quad \text{(A11)}$$

Combination of Equations A3, A5, A6, A10 and A11, and differentiation of the equations with respect to z give

$$\frac{d^2\sigma_f}{dz^2} = \frac{a^2E_f + (b^2 - a^2)E_m}{a^2E_f(1 + \nu_m)[b^2 \ln (b/a) - (b^2 - a^2)/2]} \times \left[\sigma_f - \frac{b^2E_f\sigma_0}{a^2E_f + (b^2 - a^2)E_m}\right] \quad \text{(A12)}$$

The general solution of Equation A12 is

$$\sigma_f = \frac{b^2E_f\sigma_0}{a^2E_f + (b^2 - a^2)E_m} + A \exp(\alpha z) + B \exp(-\alpha z) \quad \text{(A13)}$$

where α is given by

$$\alpha = \frac{1}{a}\left[\frac{a^2E_f + (b^2 - a^2)E_m}{E_f(1 + \nu_m)[b^2 \ln (b/a) - (b^2 - a^2)/2]}\right]^{1/2} \quad \text{(A14)}$$

and the coefficients, A and B, can be determined from the boundary conditions at the ends of the fibre. Also, the interfacial shear stress derived from Equations A11 and A13 is

$$\tau_a = -\frac{a}{2}\alpha[A \exp (\alpha z) - B \exp (-\alpha z)] \quad \text{(A15)}$$

Acknowledgements

The author thanks Drs P. F. Becher, A. Bleier and M. K. Ferber for reviewing the manuscript. Research sponsored by Division of Materials Science, Office of Basic Energy Sciences, US Department of Energy, under contract DE-AC05-84OR21400 with Martin Marietta Energy Systems, Inc.

References

1. A. KELLY and G. J. DAVIES, *Metall. Rev.* **10** (1965) 1.
2. K. M. PREWO and J. J. BRENNA, *J. Mater. Sci.* **15** (1980) 463.
3. P. F. BECHER, C. H. HSUEH, P. ANGELINI and T. N. TIEGS, *J. Amer. Ceram. Soc.* **71** (1988) 1050.
4. M. R. PIGGOTT, *Acta Metall.* **14** (1966) 1429.
5. M. R. PIGGOTT, "Load Bearing Fibre Composites" (A. Wheaton and Co. Ltd., Exeter, Great Britain, 1980).
6. A. G. EVANS and R. M. McMEEKING, *Acta Metall.* **34** (1986) 2435.
7. C. H. HSUEH, *J. Mater. Sci.*, in press.
8. *Idem, ibid.*
9. W. R. TYSON and G. J. DAVIES, *Brit. J. Appl. Phys.* **16** (1965) 199.
10. I. M. ALLISON and L. C. HOLLAWAY, *ibid.* **18** (1967) 979.
11. H. L. COX, *ibid.* **3** (1952) 72.
12. G. E. SMITH and A. J. SPENCER, *J. Mech. Phys. Solids* **18** (1970) 81.
13. A. S. CARRARA and F. J. McGARRY, *J. Compos. Mater.* **2** (1968) 222.
14. Y. TERMONIA, *ibid.* **22** (1987) 504.
15. C. H. HSUEH, *J. Mater. Sci. Lett.* **7** (1988) 497.
16. R. MUKI and E. STERNBERG, *Int. J. Solids Structures* **6** (1970) 69.
17. P. LAWRENCE, *J. Mater. Sci.* **7** (1972) 1.

Received 29 September 1988
and accepted 24 January 1989